Angular dynamical spectra. A new method for determining frequencies, weak chaos and cantori

1998 J. Phys. A: Math. Gen. 31 2913

(http://iopscience.iop.org/0305-4470/31/12/015)

J. Phys. A: Math. Gen. **31** (1998) 2913–2928. Printed in the UK PII: S0305-4470(98)86059-9

Angular dynamical spectra. A new method for determining frequencies, weak chaos and cantori

N Voglis and C Efthymiopoulos

Department of Astronomy, University of Athens, Panepistimiopolis, 157 84-Athens, Greece

Received 17 July 1997

Abstract. We define the invariant spectra of rotation angles and twist angles (angular dynamical spectra) and study the properties of their moments (angular moments) in a model two-dimensional map. The angular moments give the main frequencies of the orbits. A main frequency is defined both for a regular and chaotic orbit. For KAM curves around a centre this frequency corresponds to the rotation number. Inside islands of stability, we obtain both the main frequency (rotation number) and the 'epicyclic frequency'. A fast detection of thin chaotic layers is obtained on the basis of the behaviour of the frequency curve. We explore the resonant structure near a last KAM boundary. The secondary islands of various multiplicities, forming Farey sequences, and the noble tori between them are located. We find a criterion to determine whether various resonant chaotic zones communicate, or are separated by invariant tori.

1. Introduction

The invariant spectra of dynamical systems (dynamical spectra) were introduced in two recent papers (Voglis and Contopoulos 1994, Contopoulos and Voglis 1997). These spectra can serve as powerful diagnostic tools in dynamical systems. Several of their applications were developed in the above papers and a series of subsequent papers (Contopoulos *et al* 1995, Contopoulos and Voglis 1996, Contopoulos *et al* 1997, Voglis *et al* 1997).

In this paper a new method is presented as a direct application of the dynamical spectra, that makes possible, in a single run, the determination of the main frequencies of particular orbits, the detection of thin chaotic layers, and the location of cantori in various regions of phase space. This method is based on the calculation of spectra of *rotation angles* and *twist angles*, which will be briefly referred to as the *angular spectra* (definitions given in section 2). These spectra have an invariant character. The first spectral moments, called the angular moments, can be defined not only for regular orbits, but also for chaotic orbits. In the case of regular orbits, the angular moments give the rotation numbers of the orbits. In the case of chaotic orbits, they give a constant value in a connected chaotic domain defining a frequency characteristic of the whole domain (section 3). A fast detection of even very thin chaotic zones can be obtained, as demonstrated by numerical examples (section 4). Then we focus on the study of the phase-space structure near the last KAM boundary of an island of stability, where the method can be efficiently implemented (section 5). The stable periodic orbits of high multiplicities with rotation numbers truncations of noble numbers, their islands of stability and the noble tori between these islands are located. The destruction of a given noble torus (and the formation of a cantorus) is marked by the equalization of the angular moments of the chaotic zones on both sides of the cantorus. In summary, the method is suitable for exploring the overall phase-space structure. This structure is the

0305-4470/98/122913+16$19.50

cause of dynamical phenomena as, for example, the phenomenon of 'stickiness' and the slow diffusion of chaotic orbits.

2. Definition of the method

Consider a two-dimensional symplectic map of the form:

$$\begin{aligned} x_{i+1} &= F(x_i, y_i, a) \\ y_{i+1} &= G(x_i, y_i, a) \end{aligned} \tag{1}$$

where a is a nonlinearity control parameter. Let (x_0, y_0) be a period-1 fixed point of the map (1). Let $\bar{R}_i$ be the position vector of the point (x_i, y_i) with respect to (x_0, y_0). The *rotation angle* θ_i will be defined as the angle between the two successive vectors $\bar{R}_i$ and $\bar{R}_{i+1}$. We denote this angle as $\theta_i \equiv \mathrm{ang}(\bar{R}_i, \bar{R}_{i+1})$.

The angles θ_i can be defined in various intervals of the form $[\theta_0, \theta_0 + 2\pi)$. However, as we explain later, only some intervals are appropriate in order to avoid an unwanted constant multiple of 2π that may appear in the numerical calculations.

The spectrum of the rotation angles $S(\theta)$ is the distribution of these angles, namely:

$$S(\theta) = \frac{\mathrm{d}N(\theta)}{N\,\mathrm{d}\theta} \tag{2}$$

that is, the number $\mathrm{d}N(\theta)$ of values of θ in the small interval $(\theta, \theta + \mathrm{d}\theta)$ after N iterations.

For given initial conditions and N large enough, the spectrum $S(\theta)$ is invariant along an orbit, regular or chaotic. For example, in figures 1(a) and (b), the spectra $S(\theta)$ are shown for two orbits with initial conditions $(x_{\mathrm{in}}, y_{\mathrm{in}}) = (0.5, 0.604\,64)$ (regular) and $(x_{\mathrm{in}}, y_{\mathrm{in}}) = (1.5, 1.813\,92)$ (chaotic), in the well-studied standard map:

$$\begin{aligned} x_{i+1} &= x_i + a\sin(x_i + y_i) \qquad (x, y) \in (-\pi, \pi] \qquad \mathrm{mod}(2\pi) \\ y_{i+1} &= x_i + y_i \end{aligned} \tag{3}$$

for $a = -1.3$ (the angles θ are expressed in degrees rather than radians). The full curves in figures 1(a) and (b) are the spectra $S(\theta)$ for the first 10^6 iterations of the regular and chaotic orbits respectively, and both spectra coincide with the spectra of the same orbits for the next 10^6 iterations (dots). Thus, the spectrum $S(\theta)$ is invariant along the same orbit.

Furthermore, (a) in the case of regular orbits the spectrum $S(\theta)$ is invariant with respect to the initial conditions on the same invariant curve and (b) in the case of chaotic orbits the spectrum $S(\theta)$ is invariant with respect to the initial conditions in the same chaotic domain (Contopoulos and Voglis 1997, Contopoulos *et al* 1997).

Given the invariance of the spectrum $S(\theta)$ along an orbit, one can define the first angular moment ν_θ of the orbit as follows

$$\nu_\theta = \frac{1}{2\pi}\oint S(\theta)\theta\,\mathrm{d}\theta. \tag{4}$$

The moment ν_θ converges to a fixed value as the number of iterations increases. In fact, the fractional error $\Delta\nu_\theta/\nu_\theta$ is reduced proportionally to $1/N$, as shown, for example, in figures 1(c) and (d) for the moments of the spectra of figures 1(a) and (b) respectively.

In equation (4) we use the symbol of a closed integration with respect to the angles θ, without specifying the limits, because these limits change depending on the choice of the interval $[\theta_0, \theta_0 + 2\pi)$ of definition of θ. In order to evaluate the correct ν_θ, the interval $[\theta_0, \theta_0 + 2\pi)$ must be such that the spectrum $S(\theta)$ within this interval has no discontinuities *due to the modulo* 2π. To clarify this point, consider the spectra of figures 1(a) and (b). The spectrum 1(a) is continuous and all the angles θ belong to the interval $[0, 180^\circ]$.

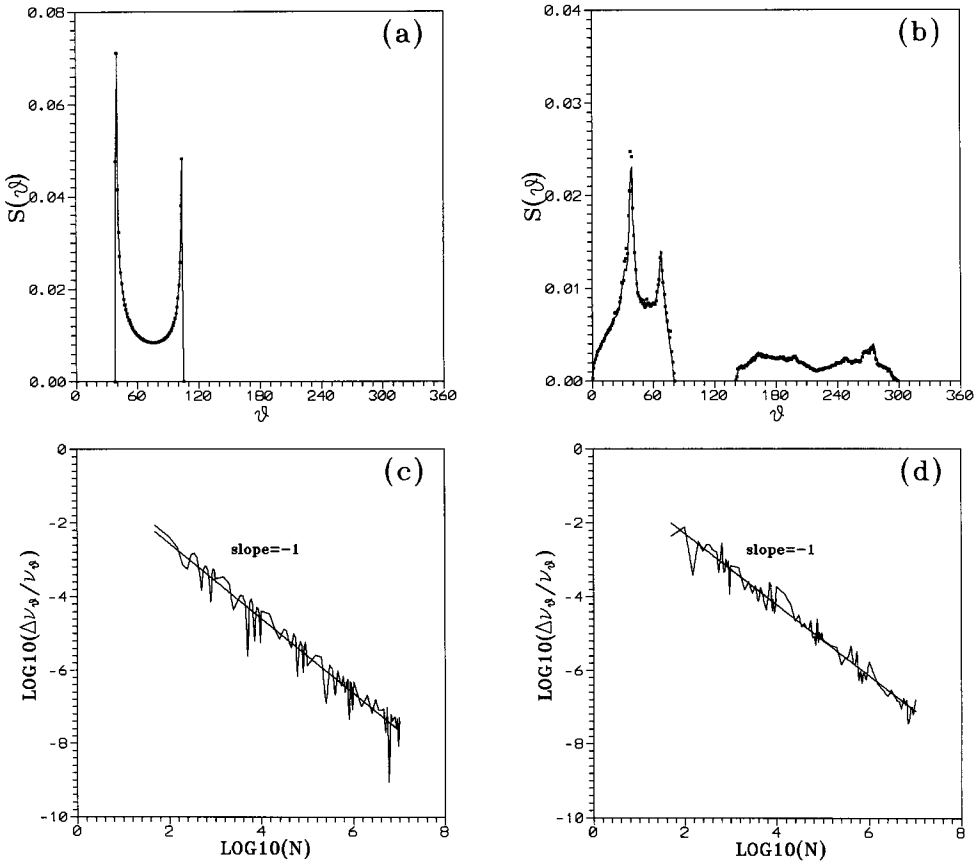

Figure 1. The spectrum $S(\theta)$ for the first 10^6 iterations (full curve) and for the next 10^6 iterations (dots) of (*a*) a regular orbit (initial conditions $x = 0.5$, $y = 0.604\,64$) and (*b*) a chaotic orbit (initial conditions $x = 1.5$, $y = 1.813\,920$) in the standard map (5) for $a = -1.3$. (*c*), (*d*) The rates of convergence of the angular moments ν_θ of the spectra (*a*) and (*b*) respectively.

On the other hand, the spectrum 1(*b*) is discontinuous, namely it has two parts separated by one gap. We call the area under the curve $S(\theta)$ 'spectral mass'. A spectral mass $m_1 \approx 70\%$ is distributed in the interval $[0, \theta_1 \cong 80^\circ]$ while the rest $m_2 \approx 30\%$ is distributed in the interval $[\theta_2 \cong 140^\circ, \theta_3 \cong 300^\circ]$. This sort of discontinuity is a real property of the spectrum, i.e. it will continue to exist independently of the choice of the interval of definition of θ. However, an improper choice of the interval of θ can produce one more 'splitting' of the spectrum, not real but only due to modulo 2π. For example, if we choose $\theta \in (-180^\circ, 180^\circ]$, then the spectral mass m_2 is now split into two disjoint parts in the intervals $[140^\circ, 180^\circ]$ and $[-180^\circ = 180^\circ - 360^\circ, -60^\circ = 300^\circ - 360^\circ]$, and the spectrum now has three disjoint parts in total, showing an apparent discontinuity at $\theta = \pm 180^\circ$. If we calculate ν_θ from equation (4) with $\theta \in [0^\circ, 360^\circ)$, we obtain the correct value, while if we adopted $\theta \in [-180^\circ, 180^\circ]$ we would obtain a different value $\nu'_\theta < \nu_\theta$ due only to the splitting of the spectrum produced by the 2π modulo.

It is possible to overcome the ambiguity due to a $2\pi-$ modulo if we define an 'extended

spectrum' $S_{\rm ext}(\theta)$ in the interval $[-2\pi, 2\pi)$ by the formula:

$$S_{\rm ext}(\theta) = \begin{cases} S(\theta) & 0 < \theta \leqslant 2\pi \\ S(\theta + 2\pi) & -2\pi < \theta \leqslant 0. \end{cases} \tag{5}$$

In the extended spectrum $S_{\rm ext}(\theta)$ there is at least one subinterval $[\theta_0, 2\pi + \theta_0)$ containing one full spectral mass ($m = 1$) without $2\pi-$ modulo discontinuities (while there may be real discontinuities). Thus, we choose this subinterval $[\theta_0, 2\pi + \theta_0)$ as the interval of integration in equation (4). If the resulting spectral moment ν_θ is negative we add 1 to obtain ν_θ in the positive interval $[0, 1)$.

For a regular orbit, the mean value ν_θ defined as above corresponds to the rotation number of the orbit. More precisely: (a) for an orbit forming an invariant curve around (x_0, y_0), the mean value ν_θ is equal to the rotation number for this curve, and (b) for an orbit inside higher-order islands around (x_0, y_0), the mean value ν_θ is equal to the rotation number of the stable periodic orbit corresponding to these islands, i.e. a rational number.

On the other hand, it is remarkable that, due to the invariance of the spectrum $S(\theta)$, a mean value ν_θ can also be defined for the chaotic orbits filling zones around (x_0, y_0) (while the rotation number of a chaotic orbit cannot be defined). Furthermore, the mean value ν_θ is the same for all the chaotic orbits belonging to one connected chaotic domain, because the spectrum $S(\theta)$ is invariant with respect to the initial conditions in the same connected chaotic domain. Thus, the mean value ν_θ of any orbit inside a connected chaotic domain defines a mean angle of rotation $2\pi\nu_\theta$ characteristic of this domain. Note that, for the reasons explained in Contopoulos and Voglis (1996), the usual ergodic theorem cannot guarantee the invariance of the spectra of chaotic orbits that we find empirically.

Nevertheless, a fundamental difficulty with the use of the angles θ and of their spectra is that their definition requires a particular choice of centre. For example, consider an orbit inside a higher-order island. If we wish to know the higher-order rotation number of the orbit around the stable periodic orbit of this island, then we must change centre and use the position of that particular stable periodic orbit as the local centre. Furthermore, in some cases, it may not be possible at all to define an obvious centre around which the rotation number is unique. This applies, for example, in many cases of irregular periodic orbits which do not bifurcate from a central periodic orbit, and, therefore, they do not define an obvious centre (Contopoulos 1970, Contopoulos *et al* 1996).

We now present a method to calculate a mean rotation number for any orbit without the need of defining any centre at all. For the map (1), the corresponding linearized map has the form:

$$\begin{aligned} \mathrm{d}x_{i+1} &= \frac{\partial F}{\partial x_i}\,\mathrm{d}x_i + \frac{\partial F}{\partial y_i}\,\mathrm{d}y_i \\ \mathrm{d}y_{i+1} &= \frac{\partial G}{\partial x_i}\,\mathrm{d}x_i + \frac{\partial G}{\partial y_i}\,\mathrm{d}y_i. \end{aligned} \tag{6}$$

We define the 'twist' angle ϕ_i as the angle by which the infinitesimal vector $\bar{\xi}_i \equiv (\mathrm{d}x_i, \mathrm{d}y_i)$ rotates in order to find the direction of $\bar{\xi}_{i+1} \equiv (\mathrm{d}x_{i+1}, \mathrm{d}y_{i+1})$. Namely, $\phi_i \equiv \mathrm{ang}(\bar{\xi}_i, \bar{\xi}_{i+1})$.

All the definitions given above regarding the rotation angles θ, the spectra $S(\theta)$, $S_{\rm ext}(\theta)$ and the first moments ν_θ can be extended in the same way to the twist angles ϕ, the spectra $S(\phi)$, $S_{\rm ext}(\phi)$ and the first moments ν_ϕ.

The spectrum $S(\phi)$ has the same invariance and convergence properties as the spectrum $S(\theta)$. For example, in figures 2(a) and (b) we have the spectra $S(\phi)$ for the first 10^6

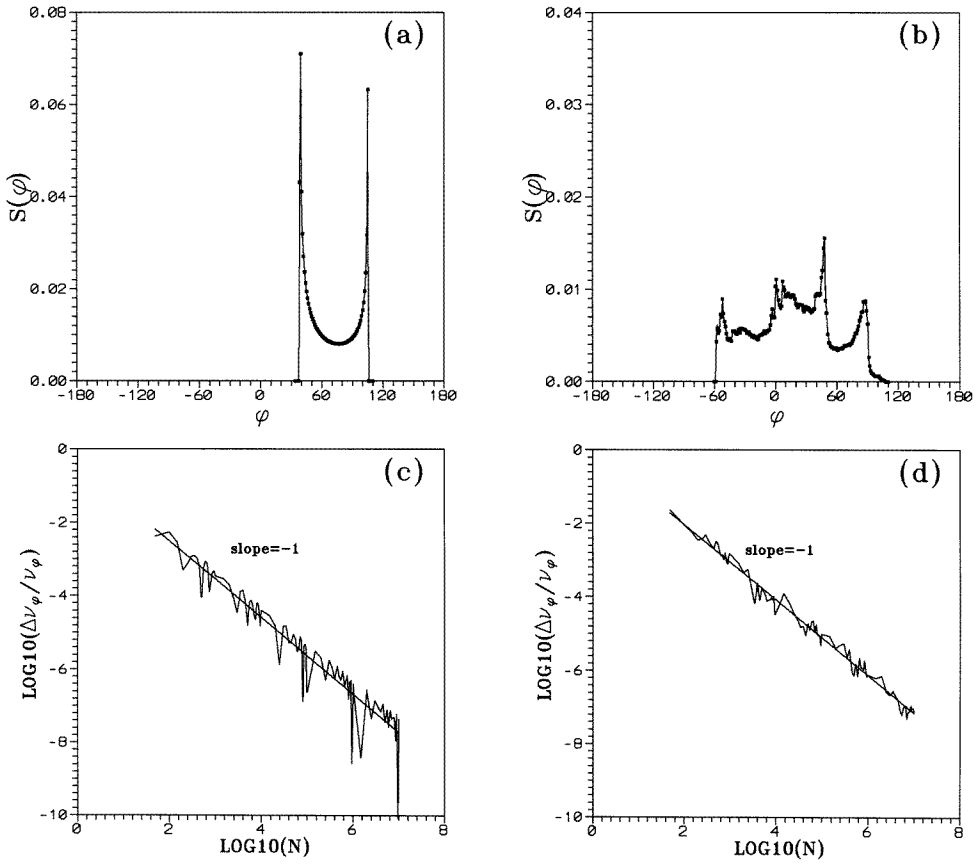

Figure 2. Same as in figure 1 for the spectra $S(\phi)$ of a regular and chaotic orbit (a), (b) and the rates of convergence of the respective angular moments (c), (d).

iterations (full curves) and for the next 10^6 iterations (dots) of the same orbits as in figures 1(a) and (b). Similarly, in figures 2(c) and (d) we plot the fractional error $\Delta\nu_\phi/\nu_\phi$ which is proportional to $1/N$.

The invariance of the spectrum $S(\phi)$ and the uniqueness of its first moment ν_ϕ are due to the fact that, independently on the initial slope of the infinitesimal vector $\bar{\xi}_0 = (\mathrm{d}x_0, \mathrm{d}y_0)$, the subsequent vectors $\bar{\xi}_i$, except the first few transient ones, tend to a unique sequence of slopes. In particular: (a) for a regular orbit on an invariant curve the vector $\bar{\xi}$ tends to become tangent to the invariant curve, and (b) for a chaotic orbit the vector $\bar{\xi}$ tends to become tangent to the unstable asymptotic curve of the simplest unstable periodic orbit (Contopoulos and Voglis 1997).

The use of the twist angles ϕ and moments ν_ϕ has the advantage that no knowledge of any centre is needed for their calculation. Only the evaluation of the linearized map is required. We now show (a) how the moments ν_ϕ of regular orbits are related to the rotation numbers of the orbits, and (b) how they can be used to locate even very thin chaotic layers.

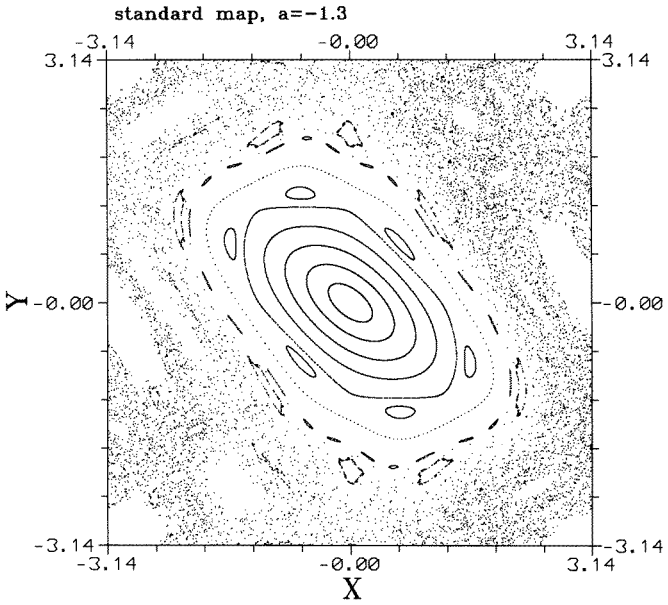

Figure 3. The phase portrait of the standard map for $a = -1.3$.

3. Determination of the rotation numbers

The phase portrait of the standard map (equation (4)) for $a = -1.3$ looks as in figure 3. The natural centre for this map is the period-1 fixed point $x_0 = 0$, $y_0 = 0$. This point is surrounded by invariant curves and by a large chaotic sea. A 6-island chain and an 8-island chain are visible while smaller island chains exist close to the boundary separating the regular from the chaotic domain.

A line of initial conditions $y = \lambda x$ is taken from the centre outwards, with $\lambda = y_6/x_6$, where $y_6 = 0.777\,07$,$x_6 = 0.642\,59$ is one of the period 6 stable fixed points. This line joins the centres $(0, 0)$ and (x_6, y_6), crossing one of the islands $\frac{1}{6}$, while it also crosses one of the islands $\frac{1}{7}$ and $\frac{1}{8}$ further out. Initial conditions in steps of $\Delta x = 10^{-4}$ are taken along the line $y = \lambda x$. The orbits are integrated for $N = 16\,384$ iterations each and the moments ν_θ and ν_ϕ for the same number of iterations are evaluated.

The curves $\nu_\theta(x)$ and $\nu_\phi(x)$ are plotted in figures 4(a) and (c) respectively, while a curve $f(x)$ giving the fundamental frequency of a fast Fourier transform on each orbit is shown in figure 4(b). Finally, in figure 4(d) all these curves are plotted together.

The curves $\nu_\theta(x)$ and $f(x)$ both have the typical behaviour of the fundamental frequency (or rotation number) curve (Contopoulos 1966, Laskar 1992). Namely, the crossing of KAM curves around $(0, 0)$ corresponds to a smooth variation of $\nu_\theta(x)$, while the crossing of an island of stability corresponds to a 'plateau' in $\nu_\theta(x)$ at the value equal to the rotation number of the island's stable periodic orbit. Finally, a chaotic domain corresponds to non-monotonic variations of $\nu_\theta(x)$, which, however, converges to a constant value in the connected chaotic domain when the number of iterations becomes larger. The curves $\nu_\theta(x)$ and $f(x)$ coincide to an accuracy of $O(1/N)$.

Consider now the curve $\nu_\phi(x)$. This curve has a parallel evolution to the curve $\nu_\theta(x)$ in the region of smooth KAM curves around $(0, 0)$. However, inside an island chain of higher multiplicity, the curve $\nu_\phi(x)$ does not give a plateau. Instead, it takes a 'U' shape. We

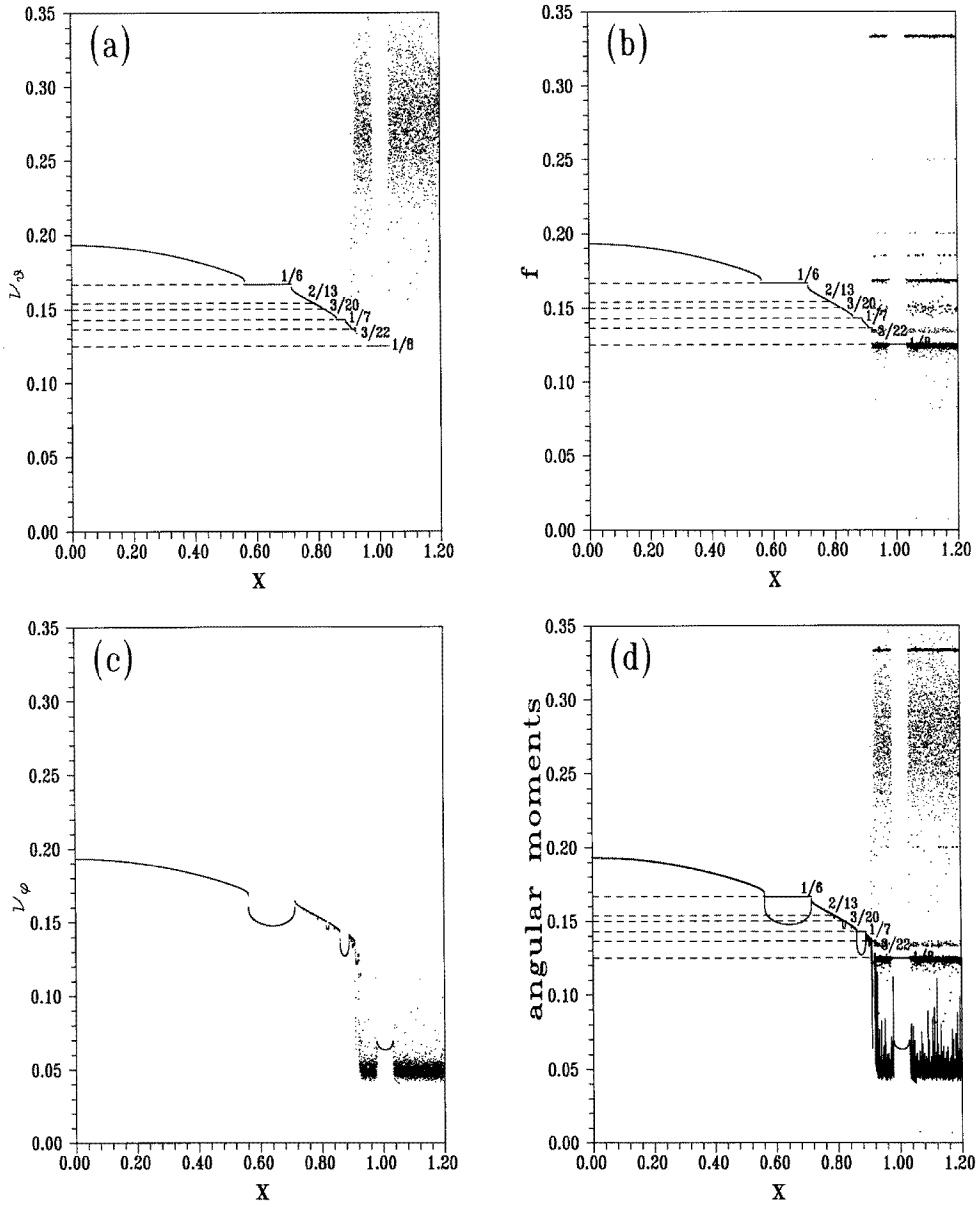

Figure 4. The curves (*a*) $\nu_\theta(x)$, (*b*) $f(x)$, (*c*) $\nu_\phi(x)$ and (*d*) a, b, c superposed, along the line $y = \lambda x$, with $\lambda = y_6/x_6$ is the slope of the line joining the centre $(0, 0)$ with one of the period 6 stable fixed points ($x_6 = 0.642\,59$, $y = 0.777\,07$).

show that this 'U' shape corresponds to the form of the curve of the 'epicyclic' frequency, that is the frequency $\nu_\kappa(x)$ or the rotation number around the local centres (the stable fixed points of higher multiplicity) of the islands. More precisely, we show that:

$$\nu_\phi = \nu_\theta \tag{7}$$

for KAM curves surrounding the central fixed point $(0, 0)$, and

$$\nu_\phi = \nu_\theta - \nu_\kappa \qquad \nu_\theta = n/m \tag{8}$$

for orbits inside islands of rotation number n/m.

Equations (7) and (8) express the following facts. (a) In the case of invariant curves around the main centre, the number of revolutions per unit time accomplished by the vector $\bar{\xi}$ around its starting point must be equal to the number of revolutions accomplished by this point around the main centre. (b) In the case of 'epicyclic' invariant curves (inside higher-order islands), the number of revolutions per unit time accomplished by the vector ξ around its starting point must be equal to the number of revolutions accomplished by the guiding centre (the island's central stable periodic orbit) around the main centre minus the number of revolutions of the starting point of $\bar{\xi}$ around the guiding centre.

3.1. Case 1: Invariant curves around the central point

In order to show equation (7), we define the angle $U_i = \mathrm{ang}(\bar{\xi}_i, \bar{R}_i)$. Then we define two differences:

$$v_i = U_{i+1} - U_i \qquad \text{(without modulo)}$$

and

$$u_i = U_{i+1} - U_i \qquad \mathrm{mod}(2\pi),\ u \in (-\pi, \pi].$$

The spectra $S(v)$ and $S(u)$ as well as their moments ν_v and ν_u can be defined in the same way as the spectra and the moments of the other angles and they have the same invariant properties.

The following equation holds:

$$\mathrm{ang}(\bar{R}_i, \bar{R}_{i+1}) = \mathrm{ang}(\bar{R}_i, \bar{\xi}_i) + \mathrm{ang}(\bar{\xi}_i, \bar{\xi}_{i+1}) + \mathrm{ang}(\bar{\xi}_{i+1}, \bar{R}_{i+1}) \qquad (\mathrm{mod}\, 2\pi) \tag{9}$$

or

$$\theta_i = \phi_i + v_i + 2\pi b_i = \phi_i + u_i \tag{10}$$

where the term $2\pi b_i$, $b_i = -1, 0, 1$ accounts for the modulo in equation (9). If we take the mean values on both sides of equation (10), where ν_ϕ is calculated through the extended spectrum $S_{\mathrm{ext}}(\phi)$, then the following equation holds:

$$\nu_\theta = \nu_\phi + \nu_u. \tag{11}$$

The time evolution of the moments ν_θ, ν_ϕ and ν_u for an invariant curve around the centre $(0, 0)$ (initial conditions $x = 0.5$, $y = 0.604\,64$) is shown in figure 5(*a*). It is observed that ν_u tends to zero as the number of iterations increases. That ν_u must tend to 0 as $N \to \infty$ can be shown as follows. Since, after a few transient iterations, the infinitesimal vector $\bar{\xi}$ becomes tangent to the invariant curve, the sequence of the angles U_i formed by the vectors $\bar{\xi}$ and $\bar{R}$ is unique, except for the first few ones. Once the vector $\bar{\xi}$ becomes tangent to the curve, the endpoint of $\bar{\xi}$ also tends to be a point of the curve. As a result, *all* the angles U_i fall into only one of the two subintervals $[0, \pi]$ or $(-\pi, 0]$ of the interval $(-\pi, \pi]$ (depending on whether the ending point of the initial $\bar{\xi}$ is inside or outside the invariant curve). Then, the two angles u_i and v_i are always equal. This means that the sum $\sum_{i=1}^{N} u_i$ is identical to the sum $\sum_{i=1}^{N} v_i$ and equal to $U_N - U_1$. This sum remains always in the interval $(-\pi, \pi]$ (figure 5(*b*)). It follows that the mean value $\nu_u \equiv \frac{1}{2\pi N}\sum_{i=1}^{N} u_i = \frac{1}{2\pi}\oint S(u)u\,\mathrm{d}u$ tends to zero $\nu_u \to 0$ as $N \to \infty$. Thus, we obtain $\nu_\theta = \nu_\phi$ (equation (7)) while the approximation of ν_θ by ν_ϕ after N iterations is of $\mathrm{O}(1/N)$.

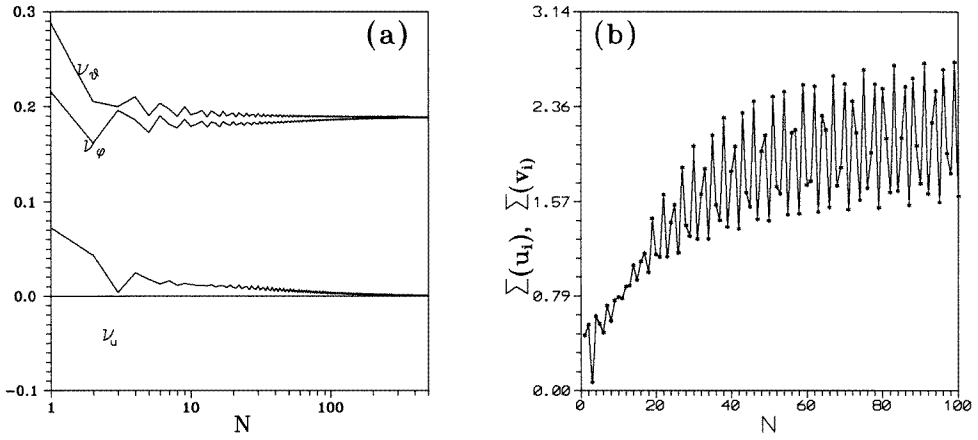

Figure 5. (*a*) The time evolution of the moments ν_θ, ν_ϕ, and ν_u for a regular orbit around $(0, 0)$ (initial conditions $x = 0.5$, $y = 0$), (*b*) the identical time evolution of the two sums $\sum_{i=1}^{N} u_i$ (full) and $\sum_{i=1}^{N} v_i$ (dots).

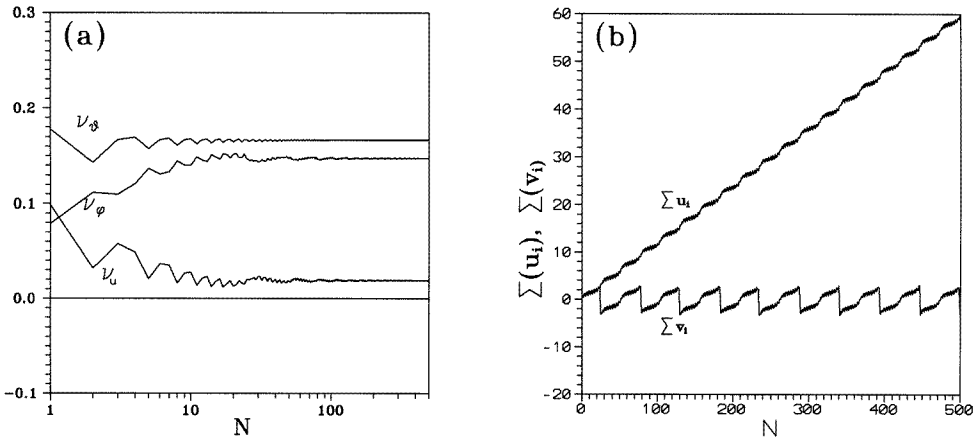

Figure 6. (*a*) The time evolution of the moments ν_θ, ν_ϕ, and ν_u for a regular 'epicyclic' orbit inside the $\frac{1}{6}$ island (initial conditions $x = 0.64$, $y = 0.773\,94$), (*b*) the time evolution of the two sums $\sum_{i=1}^{N} u_i$ and $\sum_{i=1}^{N} v_i$.

3.2. Case 2: Invariant curves inside higher-order islands

Next we consider invariant curves *inside higher-order islands* of a certain multiplicity around $(0, 0)$. Such invariant curves will be called 'epicycles'. For the epicycles, the moment ν_u does not tend to zero as $N \to \infty$. For example, in figure 6(*a*) we have the evolution of the moments ν_u, ν_θ and ν_ϕ for a regular orbit with initial conditions $x = 0.64$, $y = 0.773\,94$, inside one of the $\frac{1}{6}$ islands of figure 1. We observe that the moment ν_u converges to a limiting value different from zero. This behaviour of ν_u can be interpreted if we examine again the evolution of the sums $\sum_{i=1}^{N} u_i \equiv 2\pi N \nu_u$ and $\sum_{i=1}^{N} v_i = U_N - U_1$ with N (figure 6(*b*)). The two sums are no longer equal. The evolution of the $\sum_{i=1}^{N} v_i$ is characterized by a number of jumps of length 2π. A jump of this kind occurs each time the difference $v_i = U_{i+1} - U_i$ is outside the interval $(-\pi, \pi]$. This happens when the starting point of the vector ξ crosses

one of the tangent lines from the centre $(0, 0)$ to the epicycles. Such a crossing occurs only once per cycle of epicyclic motion (around the local island's centres). If we have k jumps after N iterations, then the ratio k/N is equal to the epicyclic frequency $\nu_\kappa = k/N$. At each jump, the difference between the two sums $\sum_{i=1}^{N} u_i$ and $\sum_{i=1}^{N} v_i$ increases by 2π. Thus, after k jumps we have:

$$\sum_{i=1}^{N} u_i = \sum_{i=1}^{N} v_i + 2\pi k \tag{12}$$

or

$$\nu_u = \frac{U_N - U_1}{2\pi N} + k/N = \nu_v + \nu_\kappa. \tag{13}$$

Since, as $N \to \infty$, $\nu_v \to 0$, we obtain $\nu_u \to \nu_\kappa$, while the actual approximation of ν_κ by ν_u is of $O(1/N)$. Thus, we obtain $\nu_\theta = \nu_\phi + \nu_\kappa$ (equation (8)). We have $\nu_\phi < \nu_\theta$ because the sense of rotation of the 'epicycle' is opposite to the sense of rotation of the main cycle of motion around $(0, 0)$. Thus the epicyclic frequency ν_κ must be substracted from the main frequency ν_θ to obtain the frequency ν_ϕ of rotation of the vector $\bar{\xi}$.

The fact that $\nu_u \to \nu_\kappa$ allows us to find the frequency ν_κ without the need to know the centres of the islands, which are periodic orbits of possibly high multiplicities. Namely, (a) we integrate the orbit and the linearized map, and (b) we evaluate the first moments ν_ϕ and ν_u. Then, $\nu_u \to \nu_\kappa$. Alternatively, we can calculate $\nu_\kappa = k/N$ by counting the number of jumps k of the function $\sum_{i=1}^{N} v_i$ after N iterations. If we add ν_u to ν_ϕ we obtain also ν_θ. In this case ν_θ is equal (within the numerical accuracy) to a rational number n/m, i.e. the rotation number of the fixed points of the islands.

With similar arguments, equation (8) can be generalized in the case of invariant curves *inside islands within islands*. In this case, we obtain the frequency of revolution of the vector $\bar{\xi}$ as a combination of the frequency ν_θ of motion around the main centre and the 'epicyclic frequencies' ν_{κ_i} around the local centres of successively higher orders. Namely, we have:

$$\nu_\phi = \nu_\theta - \nu_{\kappa 1} + \nu_{\kappa 2} - \nu_{\kappa 3} + \cdots. \tag{14}$$

In the above method, besides avoiding the calculation of the centres of the various islands, (a) no extra numerical work (e.g. Fourier analysis) is required in order to obtain the frequencies, and (b) the 'U-shape' of the curve $\nu_\phi(x)$ makes the islands more easily detectable compared with the 'plateaus' of the curve $\nu_\theta(x)$. The accuracy of this method is $O(1/N)$, although not as high as the accuracy of $O(1/N^3)$ of other methods (e.g. Laskar *et al* 1992, Lega and Froeschlé 1997), is enough when one wishes to make a fast and detailed exploration of the resonant phase-space structure, as we show by examples in the following sections.

4. Detection of thin chaotic layers

While the stable periodic orbits of various multiplicities form islands of stability around $(0, 0)$, the unstable periodic orbits of the same multiplicities produce chaotic layers forming resonant zones around the islands. These zones, especially those corresponding to periodic orbits of high multiplicities, are very thin and thus not easily detectable. In particular, the points of such chaotic zones, when seen in the usual scale, appear as forming regular curves on the plane of the map and only a great magnification reveals their non-regular structure. Furthermore, the use of traditional methods of detection of chaos fails to reveal the chaotic behaviour of the orbits in such zones within a reasonable integration time (e.g. the

convergence of the Lyapunov characteristic number of such orbits to a non-zero value may require more than 10^8 iterations, Voglis *et al* (1997)).

We can use the fact that the curve $\nu_\phi(x)$ changes slope abruptly at the crossing of each thin chaotic zone, in order to locate the accurate position of such zones along the line $y = \lambda x$ with a much smaller number of iterations per orbit. For this purpose, the calculation of the derivative function $\mathrm{d}\nu_\phi/\mathrm{d}x$ is needed. In figures 7(*a*) and (*b*) we plot the functions $\nu_\phi(x)$ and $|\mathrm{d}\nu_\phi/\mathrm{d}x|$ respectively (the function $\mathrm{d}\nu_\phi/\mathrm{d}x$ is evaluated by taking the successive differences of the function $\nu_\phi(x)$, with step $\mathrm{d}x = 10^{-4}$ and number of iterations per orbit $N = 16\,384$). The abrupt peaks of the curve $|\mathrm{d}\nu_\phi/\mathrm{d}x|$ in figure 7(*b*) mark the boundaries of the islands seen in figure 7(*a*). These peaks correspond to the thin chaotic zones which surround the islands.

5. The phase-space structrure near the last KAM curve

The study of the phase-space structure close to the boundary separating the main regular domain in figure 3 from the surrounding large chaotic domain presents a particular interest. Chaotic orbits with initial conditions outside, but very close to the last KAM curve, remain 'sticky' for a large number of periods before they diffuse into the large chaotic sea. The phenomenon of stickiness (Contopoulos 1971, Shirts and Reinhardt 1982) is due to the existence of partial barriers that limit the spreading of the chaotic orbits. The most important of these barriers are the cantori (Aubry 1978, Percival 1979, Mather 1982, Aubry and Le Daeron 1983). A cantorus is formed when a KAM torus around the island is destroyed at a critical value of the perturbation parameter. Most important are the cantori with noble rotation numbers (MacKay *et al* 1984). A noble rotation number can be represented in the form of a continued fraction approximation:

$$[a_0, a_1, \ldots] \equiv \frac{1}{a_0 + \frac{1}{a_1 + \ldots}} \tag{15}$$

with $a_i = 1$ for all i beyond some j (called the order of the noble number). Close to the gaps of a particular noble cantorus exist islands corresponding to stable periodic orbits with rotation numbers truncations of the continued fraction approximation of the noble rotation number of the cantorus. These islands also constitute temporary barriers to chaotic diffusion. In particular, they influence the form of the asymptotic curves of unstable periodic orbits inside the cantorus. As they cross one of the gaps of the cantorus, the lobes of the asymptotic curves avoid the islands near the gap. In doing so, they are forced to remain close to the cantorus for a long time after they cross the cantorus for the first time (Efthymiopoulos *et al* 1997). These lobes produce the phenomenon of stickiness.

In order to study the island structure and the formation of cantori in our example, we calculate the angular moments in the region close to the last KAM curve. We choose a new line of initial conditions passing through the centres of one of the $\frac{1}{7}$ islands ($x_7 = 0.912\,87, y_7 = 1.005\,21$) and one of the $\frac{1}{8}$ islands ($x_8 = 1.064\,97, y_8 = 1.116\,58$). For $a = -1.3$, the $\frac{1}{7}$ island is inside the last KAM curve, while the $\frac{1}{8}$ island is outside the last KAM curve, in the large chaotic sea.

In figure 8(*a*) we give the curve $\nu_\phi(s)$ (s is the distance from the fixed point x_7, y_7) along the above line of initial conditions for $N = 10^5$ iterations per orbit and scanning step $\mathrm{d}s = 10^{-5}$. Both the rotation numbers of the islands and the frequencies of the invariant tori between them are determined very efficiently with the method described in section 3.

Two domains are distinguished in figure 8(*a*) separated roughly at $s \approx 0.047$. For s greater than about 0.047 we have a large chaotic domain. For most initial conditions in

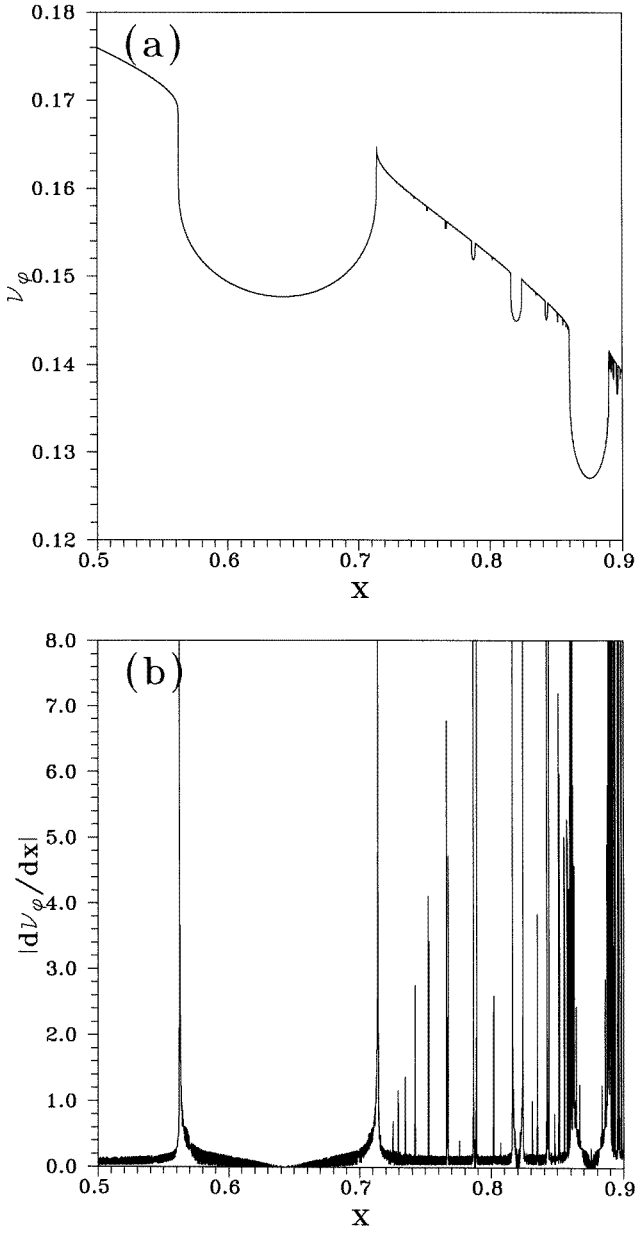

Figure 7. (*a*) $\nu_\phi(x)$ along the scanning line $y = \lambda x$ for $0.5 \leqslant x \leqslant 0.9$ and (*b*) the derivative function $|\mathrm{d}\nu_\phi/\mathrm{d}x|$ along the same line. The peaks of the derivative function mark the positions of thin chaotic layers.

this domain the moment ν_ϕ tends to a constant value $\nu_\phi \approx 0.055$, but there is also some dispersion around this value (which decreases as the number of iterations increases). The fact that the moment ν_ϕ tends to a constant value indicates that this is a *connected* chaotic domain. We can also see some islands of stability which are embedded in the chaotic domain, e.g. the islands $\frac{3}{22}$, $\frac{7}{51}$ and $\frac{2}{15}$.

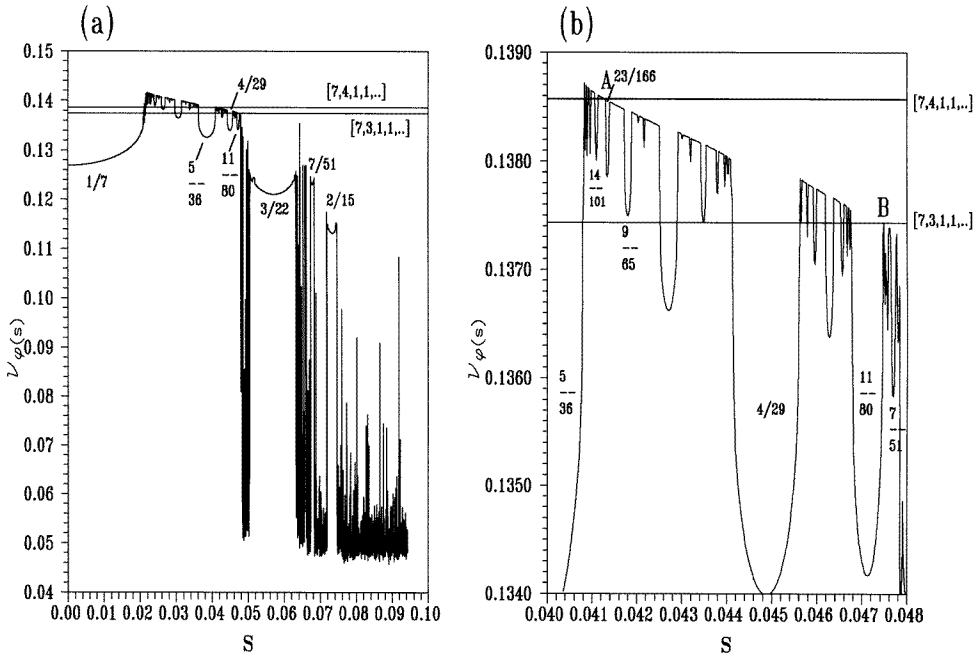

Figure 8. (*a*) The curve ν_ϕ, for $a = -1.3$ as a function of the distance s from the period 7 stable fixed point ($x_7 = 0.912\,87$, $y_7 = 1.005\,21$) along the line joining this point with the period 8 stable fixed point ($x_8 = 1.064\,97$, $y_8 = 1.116\,58$). The rotation numbers of some islands are marked, (*b*) a detail of figure 9(*a*). The points A and B belong to KAM segments and give the positions of the noble tori [7, 4, 1, 1, . . .] and [7, 3, 1, 1, . . .] respectively.

The dispersion around the constant value is not due exclusively to statistical fluctuations, but also to the phenomenon of stickiness. Namely, as long as an orbit remains 'sticky' close to the boundary separating the chaotic from the regular domain, the moment ν_ϕ takes a transient value deviating from the constant value characteristic of the chaotic domain. Nevertheless, for *all* the orbits belonging to the connected chaotic domain, ν_ϕ tends to the same value after a large enough number of iterations.

On the other hand, for s smaller than about 0.047 the curve $\nu_\phi(s)$ consists of: (a) segments that belong to a smoothly decreasing curve, corresponding to KAM tori (KAM-segments), and (b) U-shaped parts corresponding to islands. The islands form Farey sequences. For example, in figures 8(*a*) and (*b*) (detail of 8(*a*)), we see the islands with rotation numbers forming the sequence $\frac{1}{7}, \frac{4}{29}, \frac{5}{36}, \frac{9}{65}, \frac{14}{101}, \frac{23}{166}, \ldots$. These numbers are rational truncations of the continued fraction approximation of the noble number $[7, 4, 1, 1, \ldots] = 0.138\,570\,516\,109\,9319$. Similarly, the rotation numbers $\frac{1}{7}, \frac{3}{22}, \frac{4}{29}, \frac{7}{51}, \frac{11}{80}, \frac{18}{131}$, are rational truncations of the noble number $[7, 3, 1, 1, \ldots] = 0.137\,430\,725\,938\,6117$. Other islands, of which the rotation numbers are not marked in figures 8(*a*) and (*b*), belong to Farey sequences of higher-order noble numbers.

The straight lines corresponding to the noble numbers [7, 4, 1, 1, . . .] and [7, 3, 1, 1, . . .] in figure 8(*b*) intersect the curve ν_ϕ several times. The intersections at the U-shapes of islands have no special meaning. The intersections of the two lines with the curve ν_ϕ at the points A and B belong to KAM segments (in fact near B there is a small KAM segment similar to that around A). These points mark the positions of the invariant tori with the

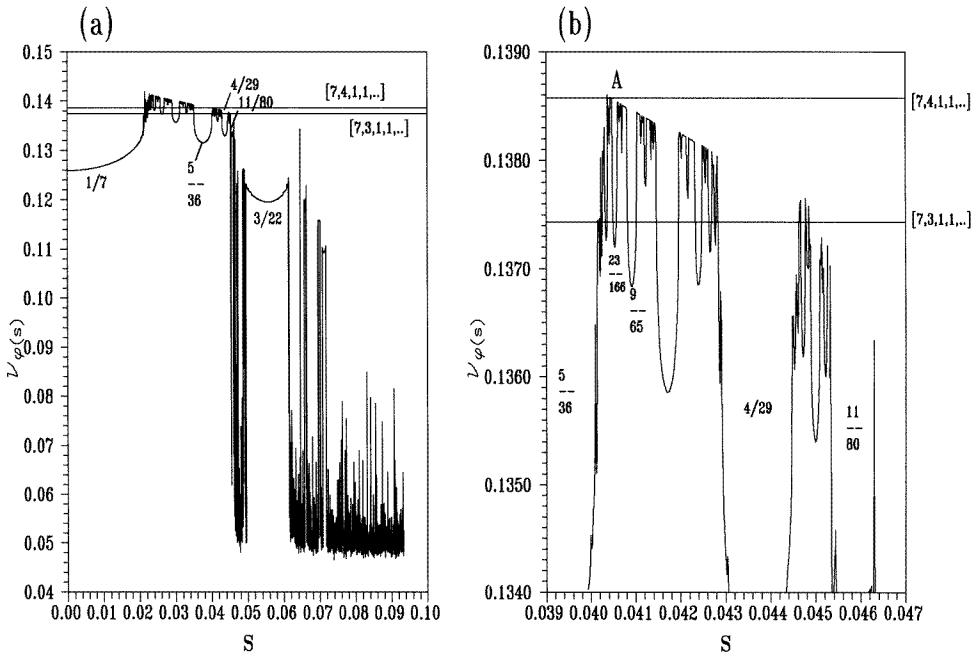

Figure 9. (*a*) Same as figure 8(*a*), for $a = -1.31$. (*b*) Same as figure 8(*b*) for $a = -1.31$. The line of the noble $[7, 3, 1, 1, \ldots]$ has no intersection with KAM segments of the curve ν_ϕ after the island $\frac{11}{80}$.

noble rotation numbers $[7, 4, 1, 1, \ldots]$ (point A) and $[7, 3, 1, 1, \ldots]$. Thus, both these tori exist for $a = -1.3$.

As we increase the perturbation, the noble tori are consecutively destroyed and become cantori. Thus, for $a = -1.31$, the noble torus $[7, 3, 1, 1, \ldots]$ has been destroyed and has become a cantorus. The destruction of the noble torus $[7, 3, 1, 1, \ldots]$ can be concluded from figures 9(*a*) and (*b*). In figure 9(*a*), we see that the connected chaotic domain has moved further to the left. Namely, there is a chaotic zone to the *left* of the island $\frac{11}{80}$ where the moment ν_ϕ has values in the constant level characteristic of the connected chaotic domain. The fact that there is communication of this chaotic zone with the large chaotic domain implies that no torus exists between $\frac{11}{80}$ and the large chaotic domain. In particular, the noble torus $[7, 3, 1, 1, \ldots]$ is destroyed. Due to the destruction of the noble torus, in figure 9(*b*) there is no intersection of the straight line of the number $[7, 3, 1, 1, \ldots]$ with a KAM segment of the curve ν_ϕ to the right of the island $\frac{11}{80}$ island, similar to the point A of the same figure.

In the same way, for $a = -1.32$, figure 10, the large chaotic domain from the right moves further to the left, including now the island $\frac{4}{29}$. In between the rationals $\frac{4}{29}$ and $\frac{11}{80}$ we have the higher-order noble $[7, 3, 1, 2, \ldots]$. Thus, for $a = -1.32$, the higher-order noble torus $[7, 3, 1, 2, 1, 1, \ldots]$ is destroyed. But besides the expansion of the right chaotic domain, we observe also the formation of a chaotic zone to the left, close to the island $\frac{1}{7}$ (region C). This zone exists also for $a = -1.31$ (figure 9(*a*)), but there it is smaller. As the perturbation increases, the width of this zone increases. This zone is separated from the outer large chaotic domain by invariant tori. As a result, the constant values of ν_ϕ are different in the two zones.

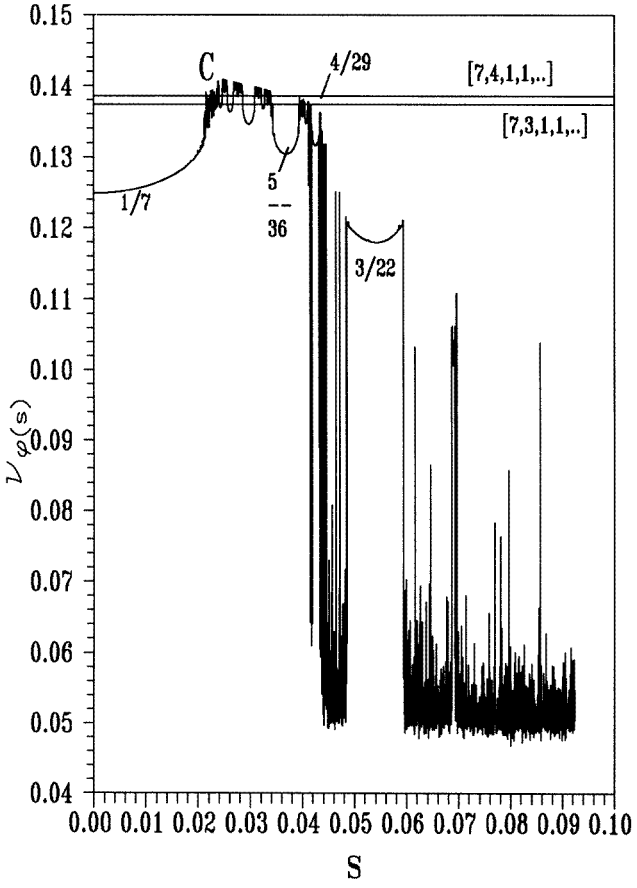

Figure 10. Same as figure 9(*a*), for $a = -1.32$.

The appearance of chaotic zones are created inside the last KAM curve and the expansion of chaos both from inside outwards and from outside inwards, is studied in detail in another paper (Efthymiopoulos *et al* 1997).

However, for a large enough perturbation, all the nobli tori are eventually destroyed and the chaotic zones between them communicate to form a large connected domain.

6. Conclusions

We have defined the rotation angles θ, the twist angles ϕ, and their respective angular spectra and moments ν_θ and ν_ϕ in a model two-dimensional map. Our conclusions are as follows.

(1) The angular spectra are invariant along one orbit, regular or chaotic. As a consequence, the angular moments can be defined in a uniform way both for regular and chaotic orbits (while the rotation number is defined only for regular orbits).

(2) The mean value ν_ϕ is equal to: (a) the mean value ν_θ (the rotation number) for regular invariant curves around the centre and (b) to the difference $\nu_\theta - \nu_\kappa$ for regular curves inside higher-order islands of stability, where $\nu_\theta = n/m$ is the rotation number of the corresponding stable periodic orbit and ν_κ is the higher-order rotation number around

the stable periodic orbit. Both of these moments can be evaluated without the need to know the centres of the islands (the points of the corresponding stable periodic orbits). The accuracy of the evaluation of the angular moments is $O(1/N)$.

(3) The peaks of the derivative function $d\nu_\phi/dx$ give the positions of thin chaotic layers. The convergence of this method, depending on the sensitivity wanted, is between 10^3 and 10^5 iterations per orbit.

(4) We explored the phase-space structure close to the last KAM boundary by using the angular moments. We located: (a) the islands forming Farey sequences, (b) the tori with noble rotation numbers and (c) the various chaotic zones formed inside and outside the last KAM curve.

(5) A connected chaotic domain corresponds to a constant mean value ν_ϕ with dispersion decreasing as the number of iterations per orbit increases. When two (or more) chaotic zones are separated by KAM tori, then the constant values of ν_ϕ in these chaotic zones are different. But when the tori are destroyed and the two zones communicate, then the values of ν_ϕ in both zones are equalized.

Acknowledgments

Stimulating discussions and critical comments by Professor G Contopoulos are gratefully acknowledged. This research was supported in part by the Greek National Secretariat for Research and Technology (PENED 293/1995). CE was supported by the Greek Foundation of State Scholarships (IKY).

References

Aubry S 1978 *Solitons and Condensted Matter Physics* ed A R Bishop and T Schneider (Berlin: Springer) p 264
Aubry S and Le Daeron P Y 1983 *Physica* **8D** 381
Contopoulos G 1966 *Paris Bull. Astron.* **2** 223
——1970 *Astron. J.* **75** 96
——1971 *Astron. J.* **76** 147
Contopoulos G, Grousouzakou E and Polymilis C 1996 *Celest. Mech. Dyn. Astron.* **64** 363
Contopoulos G and Voglis N 1996 *Celest. Mech. Dyn. Astron.* **64** 1
——1997 *Astron. Astrophys.* **317** 73
Contopoulos G, Voglis N, Efthymiopoulos C and Groussousakou E 1995 *N. Y. Acad. Sci.* **773** 145
Contopoulos G, Voglis N, Efthymiopoulos C, Froeschlé C, Gonczi R, Lega E, Dvorak R and Lohinger E 1997 *Celest. Mech. Dyn. Astron.* **67** 293
Efthymiopoulos C, Contopoulos G, Voglis N and Dvorak R 1997 *J. Phys. A: Math. Gen.* **30** 8167
Lega E and Froeschlé C 1996 *Physica* **95D** 97
Laskar J, Froeschlé C and Celleti A 1992 *Physica* **56D** 253
MacKay R S, Meiss J D and Percival I C 1984 *Physica* **13D** 55
Mather J N 1982 *Topology* **21** 457
Percival I C 1979 *Nonlinear Dynamics and the Beam–Beam Interaction* ed M Month and J C Herrera (New York: AIP) p 302.
Shirts R B and Reinhardt W P 1982 *J. Chem. Phys.* **77** 5204
Voglis N and Contopoulos G 1994 *J. Phys. A: Math. Gen.* **27** 4899
Voglis N, Contopoulos G and Efthymiopoulos C 1998 *Phys. Rev.* E **57** 372